

RECENT ADVANCES IN OTR BEAM DIAGNOSTICS*

R.B. Fiorito[#], Institute for Research in Electronics and Applied Physics, University of Maryland, College Park, Maryland, 20742, U.S.A.

Abstract

Theoretical and experimental advances in OTR diagnostics have been made over the last several years. Also, new accelerator facilities are beginning to operate in regimes where coherent effects (COTR) are being seen. COTR complicates the application of OTR for imaging but also suggests possibilities for new beam diagnostics. The state of the art of theory and experiments are reviewed and prospects for next generation of OTR diagnostics are presented.

BACKGROUND

Beam profiling, divergence and emittance diagnostics based on OTR are now common for electron and proton beam accelerators operating over a wide range of energies ranging from keV to GeV. The fast (sub ps) response, linearity to beam charge and very high spatial resolution of OTR for beam imaging have been regarded as standards for beam diagnostics and many accelerators rely on OTR screens for routine machine operations.

Imaging in particular relies on the linearity of the OTR intensity with charge. This is usually a valid assumption, since under most conditions the OTR observed is incoherent in nature, i.e. IOTR. Coherent OTR (COTR) previously has only been observed for extremely short beam pulses, which are generated by fast laser induced acceleration of charges, or by the free electron laser (FEL) or the inverse (IFEL) process operating at optical wavelengths.

Recently, however, COTR has unexpectedly been seen in new accelerators such as LCLS, which have bunch lengths much longer than optical wavelengths [1]. Since COTR has a nonlinear dependence on charge, the diagnostic beam imaging capability of OTR screens is compromised. The observation of COTR is spurring efforts to understand its cause, develop ways to suppress it and investigate its diagnostic potential.

In this paper we will give a review of contemporary diagnostic techniques based on IOTR as well as describe the properties of and observations of COTR, which have been recently reported.

INCOHERENT TRANSITION RADIATION

Transition radiation is broad band radiation emitted when a charged particle passes through a boundary between two media with different dielectric properties, e.g. a vacuum and a metal foil. The TR photons are emitted by the quickly changing charge distribution induced by the particle passing through the boundary surface. In the Weissacker Williams picture [2], the radiation from a relativistic charge, q is the reflection and

refraction of virtual photons with spectral components given by the Fourier components of the transverse field of the charge:

$$\hat{E}(\omega) = \frac{q}{\pi} \frac{\omega}{\gamma c} K_1 \left(\frac{\omega r}{\gamma c} \right) \quad (1)$$

Where K_I is the modified Bessel function. This spectrum extends up to the plasma frequency of the surface material. When the argument of $K_I = 1$, $r = b = \gamma\lambda/2\pi$, the effective transverse source size of the virtual photon with frequency ω . Here γ is the Lorentz factor of the moving charge and c is the velocity of light.

Beam Imaging with IOTR

The intensity of IOTR is rather low - about 0.001- 0.01 photons per electron in the visible band. However, because of the high current densities of modern accelerators, the high directivity of OTR for relativistic beams and the availability of sensitive, low cost cameras, OTR beam imaging is easily accomplished.

A measure of the imaging resolution of IOTR is the intensity distribution of a single charge or point spread function (PSF), which depends on the field distribution (Eq. 1) and the angular acceptance of the imaging optics, Θ . For $\Theta \gg 1/\gamma$, it has been shown [3] that

$$I_{PSF} = |E_{PSF}|^2 \sim \left[(\gamma\lambda)^{-1} K_1(r/(\gamma\lambda)) - r^{-1} J_0(r\Theta/\lambda) \right]^2 \quad (2)$$

where r is the position on the imaging plane, $D = 1/2p$ and J_0 is the zero order Bessel function [2]. The PSF is primarily sensitive to Θ and insensitive to the beam energy. Thus the width of the PSF is close to the diffraction limit of the imaging optics. As is shown in [3] the PSF has exhibits a null at $r = 0$, i.e. the intensity distribution has a donut like appearance. A comparison of images taken with IOTR and other common imaging screens such as YAG and phosphors has verified that IOTR provides the highest spatial resolution [4].

Emittance and Energy Diagnostics

For a relativistic charge incident on a highly conducting foil, the single charge spectral-angular distribution of IOTR has the form

$$\frac{d^2 I^{(S)}(\theta)}{d\omega d\Omega} = \frac{q^2}{\pi^2 c} \frac{\theta^2}{(\gamma^{-2} + \theta^2)^2}, \quad (3)$$

where $I^{(S)}$ is the intensity, ω , θ are the frequency and angle of observation $d\omega$ is the observation bandwidth and $d\Omega$ is the solid angle subtended by the detector. Note that the peak intensity of IOTR from a single interface occurs

*Work supported by ONR and the DOD Joint Technology Office
[#]rfiorito@umd.edu

at the angle $1/\gamma$, and the intensity of IOTR is independent of the frequency. This expression is only valid for frequencies much lower than the plasma frequency of the foil material, which is usually the case.

The *angular distribution* (AD) of IOTR, which can be simply determined from Eq. 3, is useful to measure the energy, divergence and, in combination with imaging, the rms emittance of a relativistic charged particle beam [5]. For a charge incident on a foil oriented at 45 degrees with respect to the velocity of the charge, forward and backward OTR are generated. The AD of the former is centered about the velocity vector; the latter, about the direction of specular reflection.

To measure the divergence using the AD of IOTR, a model for the distribution of beam charge trajectory angles, e.g. a Gaussian function, is chosen and then convolved with Eq. 3. The result produces a function of the distribution width and observation angle, which when fit to the data, produces the rms divergence. For a non axisymmetric case, two Gaussians with corresponding rms (x' , y') divergences are used to model the angular distribution of the charges and to do the fitting.

For greater sensitivity to beam parameters, an OTR interferometer, consisting of two parallel foils, which are oriented at 45° and separated by distance L , is used. The interference of forward directed OTR generated from the rear of the first foil interferes with backward OTR generated from the second mirror foil. The expression for the intensity is Eq. 3. multiplied by $4\sin^2(\phi/2)$, where $\phi = L/L_V(\gamma, \lambda, \theta)$ is the relative phase between the photons generated at the two surfaces and L_V is the vacuum coherence length of the radiation. For a high γ beam the interferences are observed in reflection, i.e. by viewing between the foils.

To avoid compromising the measurement, the first foil must be thin enough so that the scattering in the foil does not significantly increase the emittance; also the energy spread of the beam must be much lower than the normalized *rms* divergence ($\gamma\theta_{rms}$). The fringe visibility is then a measure of the beam divergence [6].

To further overcome the limitation of beam scattering we use a micromesh first foil of the interferometer. In this case optical diffraction radiation (ODR) is produced in the mesh when the hole size is comparable to $b = \gamma\lambda/2\pi$. The material and thickness of the wires of the mesh are purposely chosen to produce large scattering angles from charges intercepting the mesh wires. In this case the unscattered charges produced fringes which ride above an IOTR background produced by the scattered charges [7].

To extend the range of measurement to lower energy beams which demand a small inter foil spacing (L_V mm), we have developed a novel transmission interferometer which employs a micromesh and a transparent dielectric foil [8, 9]. This configuration allows us to observe the interference of forward directed radiation from the two foils transmitted through the dielectric foil.

For emittance measurements two cameras are used, one focused on the mirrored foil to measure the rms beam size, the other focused at infinity to observe the AD and measure the rms divergence. In order to determine the normalized rms emittance

$$\tilde{\epsilon}_x^2 = \beta^2 \gamma^2 (\langle x^2 \rangle \langle x'^2 \rangle - \langle xx' \rangle^2), \quad (4)$$

from a simple product of these two observables, the beam must be magnetically focused to a waist condition where the correlation term $\langle xx' \rangle = 0$. This is usually difficult to achieve in practice and as an approximation one usually focuses the beam to a minimum radius in either the x or y in order to measure the corresponding divergence. In previous experiments, the rms emittances obtained by taking the simple product of the rms values of (x, x') or (y, y') measured at a corresponding focus, have compared favourably with independent measurements. These results indicate that the correlation terms were small in these experiments.

However, it is well known [10] that the beam size at a magnetic focus does not necessarily occur at, nor is it equal to, the 'true' beam waist, i.e. the minimum in the beam envelop as a function of *position* along the beam line for a fixed setting of the focusing field. Therefore, in to improve the diagnostic technique and make it generally applicable, we have developed algorithms which relate the correlation term to the beam size minimum or the beam divergence minimum. These values can be measured by performing quadrupole scans in either variable [9]. With these new algorithms it is now possible to determine rms emittance with greater accuracy and for more diverse beam conditions.

Optical Phase Space Mapping (OPSM)

A general technique for optically mapping the transverse phase space of a charged particle beam has been developed using OTR [11]. OPSM can be used with any type of beam based radiation and does not require that the beam be at waist. We will give a brief synopsis of the method using OTR.

The OTR from a foil or interferometer mirror is first imaged onto a plane which contains an optical mask to selectively block or pass a segment of the beam image. The AD of the OTR passing through the mask, e.g. an aperture, can be used to measure the local divergence and trajectory angle within a portion of the image. For example, we have scanned a pinhole over the OTR image of a 100 MeV e beam to create x, x' and y, y' maps of the beam.

An extension of this idea uses an adaptive mask based on a digital micro-mirror array (DMA) to for beam halo studies [12]. Fig. 1. shows test results obtained using DMA with a HeNe laser beam first to observe the entire intensity profile and then the halo. To do this the DMA is programmed to eliminate all points on the image with intensities exceeding a set level. The advantages of this technique are: 1) programmable mask geometry; 2) high speed (10 μ sec) digital control at the pixel level; and 3)

high extinction ratio (10^5) between masked and unmasked portions of the image.



Figure 1: Left: picture of HeNe laser imaged onto a DMA with a defined core specified by the red oval overlay; right: same picture with core light removed.

Fluctuation Bunch Length Diagnostics

A number of studies originating with [13] have shown that the bunch length of a beam can be measured by analyzing fluctuations in the intensity of incoherent optical synchrotron radiation (IOSR). Recently it was further demonstrated that the absolute rms bunch length can be obtained by measuring the variance of the fluctuations from many bunches observed in a narrow optical band pass [14]. Comparison of bunch lengths of the ALS synchrotron at LBNL measured with this method and a streak camera show excellent agreement.

It should be noted that (a) fluctuations of any beam radiation process including OTR can be used; and (b) fluctuations occur even in the coherent portion of the spectrum. The latter are typically not observable because the variances are usually orders of magnitudes smaller than in the incoherent part of the spectrum. However, we shall see below that such fluctuations are observed in the visible part spectrum of COTR at LCLS. These fluctuations may be useful as a bunch length diagnostic.

COHERENT TRANSITION RADIATION

COTR has recently been observed in the SLAC-LCLS and other electron beam accelerators. The observation of COTR has been attributed to micro-bunching at optical wavelengths. These modulations arise from longitudinal density fluctuations (shot noise). Linear space charge forces convert these to energy modulations which then produced amplified micro bunches in magnet bends and bunch compressors [15].

A number of diagnostic experiments have been done to study the spatial and spectral features of the observed COTR. We will first discuss the general properties of coherent transition radiation (CTR); then the features of COTR produced in circumstances where it is expected and has been observed previously; and finally COTR which has unexpectedly been observed.

CTR Diagnostics

Observation of the spectral properties of CTR at wavelengths $\lambda \geq \sigma_z$ the longitudinal beam size, have been used for many years to diagnose the bunch length of charged particle beams. The basis of the method can be

seen from an analysis of the spectral angular density of CTR given by

$$\frac{d^2 I}{d\alpha d\Omega} = \frac{d^2 I^{(s)}}{d\alpha d\Omega} \{N + N(N-1) f_{\perp}(k_{\perp}, \sigma) f_z(k_z, \sigma_z)\}, \quad (5)$$

where, I is the intensity of the total radiation observed from N particles, $I^{(s)}$ is the radiation from a single particle given by Eq. 1, $f_{\perp, z} = |F(\rho_{\perp, z})|^2$ are the squared absolute values of the Fourier transforms of the transverse (\perp) and longitudinal (z) charge distributions and σ is the transverse beam size. When multiplied by the first term, the second and third terms on the RHS of Eq. (5) are the spectral angular densities of the incoherent and coherent radiation intensities (I_{incoh} , I_{coh}). The degree of coherency or coherent gain is defined by $G = I_{coh} / I_{incoh} = N f_{\perp} f_z$.

For a radiator size $D \gg b$, $I^{(s)}$ does not depend on frequency. In this case the frequency dependence of the form factors determines the spectral density of the CTR. By measuring the spectrum of the CTR, either directly or with an autocorrelation method [16], the bunch length and in some cases the longitudinal distribution can be determined.

Note, however, if $b \geq D$, diffraction effects introduce a frequency dependence into $I^{(s)}$. These effects as well as frequency dependences introduced by the transport optics and detector response must be carefully taken into account in the analysis [17].

COTR Imaging

The intensity distribution from an ensemble of charges intercepting a screen can be found by squaring the coherent sum of the radiation fields observed at the imaging plane. This can be done by directly or analytically as in [1], where it has been shown that the intensity distribution at the image plane can be approximated as the sum of 1) an incoherent intensity, equal to N multiplied by the convolution of the charge density with the single particle intensity (i.e. the normal IOTR image intensity discussed above); and 2) an coherent intensity, which is proportional to N^2 times the square of the convolution of the particle distribution with the single particle *field* on the foil. The latter, which dominates if $G > 1$, is not directly proportion to the charge density distribution of the beam.

The COTR image intensity distribution depends on the ratio of the transverse beam size σ to the effective source size of a single electron b . There are two regimes:

- 1) $\sigma < b$; here, the COTR image is just the convolution of the PSF with the beam charge distribution or, in the extreme case when $\sigma \ll b$, is just equal to the PSF; and
- 2) $\sigma > b$; here, the COTR image is equal to the transverse gradient of the charge distribution.

As an example, Fig. 2. shows our calculations of the normalized line profiles of the COTR image intensity for an axisymmetric Gaussian beam charge distribution with

rms width $\sigma = 200$ microns and beam energy $E = 250$ MeV - the LCLS parameter just after the first bunch

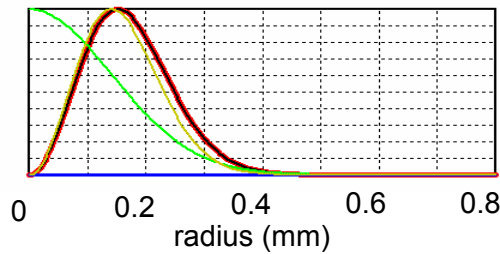


Figure 2: Line profiles of an axial symmetric Gaussian beam distribution (green), the transverse gradient of the distribution (yellow); and COTR intensity distribution (red).

compressor (BC1). For comparison we show the beam density profile and the transverse gradient of the distribution as well. These results indicate that the COTR distribution is close to the gradient of the Gaussian for these beam conditions.

An actual OTR screen image observed at LCLS just after BC1 is shown in Fig. 3. along with a horizontal wire scan taken close to the screen. The COTR intensity in this image is about 100 times more intense than the IOTR observed before the DL.

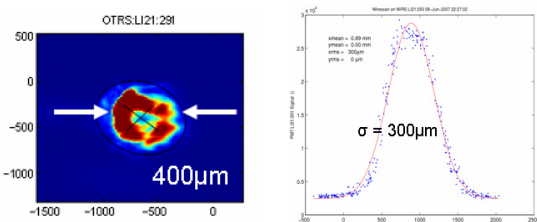


Figure 3: Left: COTR image 1; right: horizontal wire scan across the center of the beam; from [1].

A line scan across the beam image shows a null in the center of the profile. The wire scanner data shows a smooth nearly Gaussian distribution. The peak intensity in the image occurs at about $150 \mu\text{m}$ from the center of the image which corresponds to the half width of the wire scan distribution, in accord with the calculations of the transverse gradient shown in Fig. 2.

Images obtained after the second bunch compressor at LCLS at 4.3 GeV shows a stronger COTR production ($\sim 10^5$ IOTR) and an image intensity distribution that also agrees with theoretical prediction for $\sigma < b$. In this the COTR image is also 'donut'-like similar to Fig. 3. However, in this case the effect is due to the PSF and is not the gradient of the beam distribution.

CTR Spectra

CTR in the FIR, mm and optical regime have been observed previously in beams which are modulated by the free electron laser (FEL) [18] or the inverse process

(IFEL) [19]. In a FEL the interaction of the beam with the wiggler directly produces the density modulation. In an IFEL, an energy modulation is first imposed by a laser, which is then converted into a density modulation as the beam passes through a chicane. In each case periodically spaced micro-bunches are formed in the longitudinal charge distribution at the wiggler (FEL) or laser wavelength (IFEL). The CTR from n micro-bunches interfere resulting in lines in the spectrum at the harmonics of the modulation frequency [20].

The spectrum of IOTR and COTR has been measured at LCLS by placing a transmission grating in front of the OTR foil station CCD camera after BC1. The resolution (6 nm) is limited by the beam size image size on the grating. The results are presented in Fig 4. taken from [1]. The data is taken for a nominal bunch length of $60 \mu\text{m}$.

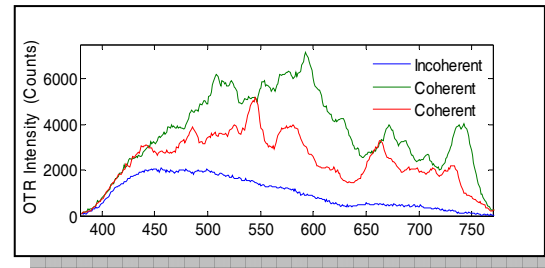


Figure 4: Comparison of COTR spectrum of two individual shots (red and green plots) with BC1 and IOTR with BC1 off; axis is wavelength in units of nanometers.

In contrast to the periodic microbunching processes described above, the spectrum of the COTR at LCLS exhibits apparently random shot to shot fluctuations. This result is consistent with what is expected from the microbunching instability and a plot of gain G vs. wavelength shows that the intensity grows exponentially. Remarkably, a fit of theoretical gain curves to the experimental data requires only one free parameter, the slice energy spread. For the best fit, this parameter is 3keV, a value which is consistent with what is expected for the LCLS photocathode RF gun [15].

Mitigation of COTR

Several schemes have been proposed to mitigate COTR. These include: wavelength filtering [21]; introduction of a scattering foil, which has the effect of destroying the coherence by increasing the divergence [22]; and spatial filtering in the Fourier plane, which we will discuss here.

Fig 5. shows the normalized AD's of IOTR and COTR for the same beam parameters used in Fig. 2. Note that the COTR has a much narrower angular distribution than the IOTR, which peaks at $1/\gamma$. This effect is formally due to the transverse form factor (see Eq. 5), which for a Gaussian beam, is $f_{\perp}(\sigma, k_{\perp}) = \exp[-(\pi\sigma \sin \theta / \lambda)^2]$.

This term severely truncates the AD of the COTR in comparison to IOTR when $\sigma > b$ and $\theta \sim 1/\gamma$. A more physical interpretation is that the effective size of the

COTR source is the entire transverse beam size σ , when $\sigma > b$. This larger coherent radiator, which contains N charges, produces a greater directivity of COTR in comparison to IOTR, which is produced by N incoherent radiators with the same effective source size (b) and AD.

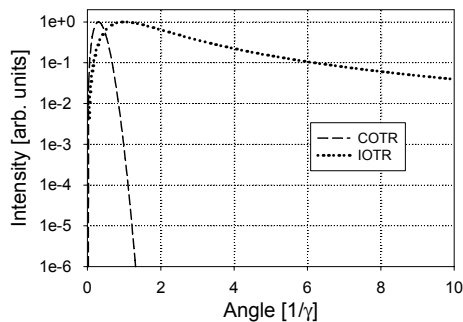


Figure 5: Far field angular pattern of IOTR and COTR.

The Fourier plane filtering method that we propose is done by placing a blocking stop in the focal plane of the lens used to image the far field AD. When the angular half width subtended by the stop is sufficiently large, the COTR can be decreased by many orders of magnitude. The IOTR outside the angular range of the stop can then be used to image the beam. Fig. 5. shows that this method should work well for LCLS at 250 MeV. But it becomes more difficult at very high energies e.g. 4.3 GeV, where the AD's of IOTR and COTR overlap to a greater extent at angles near $1/\gamma$.

CONCLUSIONS

We have examined the properties of incoherent and coherent transition radiation which are useful as well as problematic for beam diagnostic applications. The COTR observed is thought to result from chaotic micro bunching at optical wavelengths. New methods are being developed to both mitigate and utilize COTR as a new diagnostic.

REFERENCES

[1] H. Loos, R. Akre, A. Brachmann, et. al., "Observations of Coherent Transition Radiation in the LCLS Linac", THBAU01, FEL08, Gyeongju, Korea Aug. 2008; and SLAC-PUB-13395, Sept. 2008.
 [2] J. Jackson, Classical Electrodynamics, 3rd Ed., J. Wiley, NY (1999).
 [3] D. Xiang, W. Huang and Y. Lin, Phys. Rev. ST Accel. and Beams 11, 062801 (2007).
 [4] A. Murokh, J. Rosenzweig, I. Ben-Zvi, X. Wang, and V. Yakimenko, "Limitations on Measuring Transverse Profiles of Ultra Dense Electron Beams with Scintillators", Proc. of PAC01, 2, 1333 (2001).
 [5] R. Fiorito and D. Rule, "OTR Beam Emittance Diagnostics", AIP Conf. Proc. 319, 21, (1994).
 [6] M. Holloway, R. Fiorito, A. Shkvarunets, P.O'Shea, S. Benson, D. Douglas, P. Evtushenko and K. Jordan,

Phys. Rev. ST Accel. and Beams, 11, 082801, (2008).
 [7] R. Fiorito, A. Shkvarunets, T. Watanabe, V. Yakimenko and D. Snyder, Phys. Rev. ST Accel. and Beams, 9, 052802 (2006).
 [8] A. Shkvarunets, R. Fiorito, P. O'Shea, M. Conde, W. Gai and J. Power, "Optical Diffraction-Dielectric Foil Radiation Interferometry Divergence Diagnostics for Low Energy Electron Beams", FRPMS034, Proc. of PAC07, Albuquerque, NM, June 2007.
 [9] C. Papadopolous, R. Fiorito, R. Kishek, P. O'Shea, A. Shkvarunets, J. Power, M. Conde and W. Gai, "Determination of True RMS Emittance from OTR Measurements", TH6REP053, these Proceedings.
 [10] M. Reiser, Theory of Charged Particle Beams, 2nd Ed., Wiley, NY (2008).
 [11] R. Fiorito, A. Shkvarunets and P. O'Shea, "Optical Method for Mapping the Transverse Phase Space of a Charged Particle Beam", AIP Conf. Proc. 648, 187 (2002).
 [12] J. Egberts, S. Artikova, C. Welsch, "Flexible Core Masking Technique for Beam Halo Measurements with High Dynamic Range", Proc. of DIPAC09, Basel, Switzerland, May 25-27, 2009; see also C. Welsch, E. Bravin, T. Lefevre, "A Beam Halo Monitor Based on Adaptive Optics", Proc. of the SPIE, Vol. 6616, p. 66160M (2007).
 [13] M. Zolotarev and G. Stupakov, "Fluctuational Interferometry for Measurement of Short Pulses of Incoherent Radiation", SLAC-PUB-7132, Mar. 1996.
 [14] F. Sannibale, G. Stupakov, M. Zolotarev, D. Filipetto and L. Jaegerhofer, Phys. Rev. ST Accel. and Beams, 12, 032801 (2009).
 [15] D. Ratner A. Chao and Z. Huang, "3D Analysis of Longitudinal Space Charge Microbunching Starting from Shot Noise", TUPPH041, FEL08, Gyeongju, Korea, Aug. 2008.
 [16] H. Lin, P. Kung, C. Settakorn and H. Wiedemann, Phys. Rev. Lett. 53, 6413 (1996).
 [17] A. Shkvarunets and R. Fiorito, Phys. Rev. ST Accel. and Beams 11, 012801 (2008) and references therein.
 [18] A. Lumpkin, R. Delius, J. Lewellen, et. al., Phys. Rev. Lett. 88, 234801, (2002)
 [19] C. Sears, E. Colby, R. Ischebeck, et. al., Phys. Rev. ST Accel. and Beams 11, 061301 (2008).
 [20] J. Rosenzweig, A. Tremaine and G. Travish, Nuc. Instrum. and Methods A 365, 255 (1995).
 [21] A. Lumpkin, W. Berg, Y. Li, S. Pasky and N. Sereno, "Mitigation of COTR due to the microbunching instability in compressed beams", TH5RFP043, these Proceedings.
 [22] A. Murokh, E. Hemsing, J. Rosenzweig, "Multiple Scattering Induced Mitigation of COTR Emission from Microbunched Electron Beams", Paper TH6REP021, these Proceedings.